Research Square

Preprints are preliminary reports that have not undergone peer review.
They should not be considered conclusive, used to inform clinical practice,
or referenced by the media as validated information.

Integrating satellite observations and spatial data for comparative urban NO_2 analysis through a web-based geospatial platform

Jonas Olbrich
University of Augsburg
Michael Wurm
German Aerospace Center (DLR), Earth Observation Center (EOC)
Cesar Ivan Alvarez
cesar.alvarez@uni-a.de

University of Augsburg

Research Article

Keywords: NO_2, Sentinel-5P, TROPOMI, Geospatial information systems, Urban air pollution, WebGIS

Posted Date: November 25th, 2026

DOI: https://doi.org/10.21203/rs.3.rs-11839345/v1

License: This work is licensed under a Creative Commons Attribution 4.0 International License.
Read Full License

Additional Declarations: No competing interests reported.

Title

Integrating satellite observations and spatial data for comparative urban NO_2 analysis through a web-based geospatial platform

Author names and affiliations

Jonas Olbrich[a], Michael Wurm[b], and Cesar Ivan Alvarez[c,*]

[a] Institute of Geography, Faculty of Applied Computer Science, University of Augsburg, Augsburg, Germany

[b] German Aerospace Center (DLR), Earth Observation Center (EOC), Oberpfaffenhofen, 82234, Germany

[c] Centre for Climate Resilience, University of Augsburg, Universitätsstraße 12a, 86159 Augsburg, Germany

Email address list:

Jonas Olbrich: jonas.olbrich@uni-a.de

Michael Wurm: Michael.Wurm@dlr.de

Cesar Ivan Alvarez: cesar.alvarez@uni-a.de

***Corresponding author:**

Cesar Ivan Alvarez

Centre for Climate Resilience, University of Augsburg, Universitäts Strasse 12a, 86159 Augsburg, Germany

e-mail: cesar.alvarez@uni-a.de

Tel. : +4915225379102

Abstract:
Satellite observations provide extensive information on atmospheric pollution, but comparing cities requires consistent spatial units, temporal records and analytical indicators. This study presents a web-based geospatial platform integrating Sentinel-5P tropospheric NO_2 observations, urban spatial data and statistical analysis for 288 selected cities across six continents. Monthly observations from June 2018 to August 2026 were processed using Google Earth Engine and organized into linked monthly, annual and seasonal records in PostgreSQL/PostGIS. A Django/GeoDjango application enables interactive comparisons of geographical distributions, estimated trends and seasonal variability without repeating satellite extraction. The results showed substantial differences in tropospheric NO_2 columns, with a median long-term value of 37.8 μmol m^{-2} and a range of 2.8–386.2 μmol m^{-2} across the selected cities. Annual trends also varied geographically: 34 cities showed nominal increases and 16 nominal decreases, although none remained significant after correction for multiple comparisons. Restricting the analysis to complete calendar years reduced nominal detections from 50 to 23, showing the sensitivity of trend classifications to temporal coverage. Seasonal profiles further revealed contrasting patterns between tropical and extratropical cities. These findings show the importance of examining atmospheric NO_2 levels alongside temporal variability and statistical uncertainty rather than relying on individual indicators. By integrating satellite observations, spatial databases, and interactive analysis, the platform provides an integrated approach to comparing urban atmospheric conditions and supporting further investigation of environmental patterns across cities, with open access for other research and applications.

Keywords:
NO_2; Sentinel-5P; TROPOMI; Geospatial information systems; Urban air pollution; WebGIS

1. Introduction

Nitrogen dioxide (NO_2) is an atmospheric pollutant associated with combustion processes, particularly road transport, industrial activities and energy production. Its distribution in urban environments is influenced by emissions, atmospheric transport, chemical reactions and meteorological conditions. Understanding its spatial and temporal variability is therefore important for investigating changes in urban atmospheric pollution. The TROPOspheric Monitoring Instrument (TROPOMI), onboard Sentinel-5P, provides frequent observations with broad geographical coverage, enabling the examination of NO_2 patterns across cities with different environmental and socioeconomic conditions (Veefkind et al. 2012; van Geffen et al. 2022; Verhoelst et al. 2021). Although satellite-derived tropospheric columns do not directly represent near-surface concentrations or population exposure, remote sensing observations can complement conventional air-quality monitoring, particularly in regions where ground-based measurements are sparse or unavailable (Alvarez-Mendoza et al. 2019). Their geographical coverage offers additional opportunities to investigate atmospheric variability, identify monitoring gaps and support environmental assessments in areas where local observations alone provide limited information.

Previous studies have documented global and regional changes in atmospheric NO_2 using satellite observations (Geddes et al. 2016; Krotkov et al. 2016; Fioletov et al. 2025). More recent investigations have examined relationships between urban development and atmospheric pollution (Wurm et al. 2025), changes in NO_2 across more than 11,000 urban areas (Huber et al. 2026), and meteorologically adjusted trends across several thousand cities (Hassani et al. 2026). Regional studies have also investigated differences between urban and surrounding background conditions and their relationships with environmental characteristics (Alvarez et al. 2026). These investigations provide extensive evidence of geographical and temporal differences in urban atmospheric NO_2. Nevertheless, comparing cities remains challenging because urban boundaries, monitoring availability, population characteristics and local atmospheric conditions differ substantially. Consistent geographical definitions and temporal indicators are therefore needed to examine these differences within a common analytical framework, while retaining the information required to interpret individual cities.

Developments in cloud computing and geospatial information technologies have facilitated broader access to Earth Observation data and their application to environmental monitoring. Google Earth Engine (GEE), for example, provides access to extensive satellite archives and supports the processing of observations across large geographical areas (Gorelick et al. 2017). Applications developed for Ecuador (Alvarez-Mendoza et al. 2023) and South Africa (Shikwambana et al. 2025) have demonstrated how satellite-derived air pollution information can

be explored through web-based interfaces. Beyond data visualization, connecting satellite observations with spatial databases and statistical tools allows users to examine geographical distributions, temporal changes and seasonal variability using consistent spatial references. This is particularly relevant for environmental agencies and researchers working in regions with limited monitoring infrastructure, where accessible information can help identify locations requiring further investigation. Such developments also contribute to broader efforts to improve the organization, accessibility and reuse of multidimensional Earth Observation datasets (Mahecha et al. 2020; Wilkinson et al. 2016; Scheick et al. 2026).

This study develops and applies a geospatial information workflow to examine tropospheric NO_2 observations across 288 cities worldwide using Sentinel-5P data from 2018 to 2026. Three questions guide the analysis: (i) how can urban boundaries, satellite observations and temporal indicators be connected within a common geospatial information system; (ii) what geographical and temporal patterns emerge when NO_2 levels, trends and seasonal variability are examined together across cities; and (iii) how does temporal coverage influence the interpretation of these indicators? The workflow integrates satellite data extraction, spatial database management, statistical analysis and interactive visualization, allowing cities to be compared through a common set of observations and analytical procedures. The study also examines how these comparisons can help identify cities with elevated NO_2 columns or changing atmospheric conditions that may warrant closer environmental assessment. Rather than treating all cities as directly equivalent, the approach provides a common analytical starting point while recognizing differences in their geographical settings and urban characteristics. The resulting information can support future monitoring efforts and the integration of additional environmental and socioeconomic data relevant to urban planning and public health research.

2. Materials and methods

2.1 Processing and information architecture

The study was implemented through a five-stage geospatial information workflow (Fig. 1): (i) acquisition and preparation of satellite and contextual data; (ii) extraction of city-level NO_2 observations using Google Earth Engine (GEE); (iii) temporal aggregation and statistical analysis in Python; (iv) management of spatial and temporal records in PostgreSQL/PostGIS; and (v) interactive analysis and visualization through Django/GeoDjango.

The workflow separates satellite processing from data storage and subsequent analysis. Each city is assigned a persistent identifier that links its geographical location, urban footprint, demographic attributes and monthly, annual and seasonal NO_2 observations. These relationships are maintained

in the database, while statistical indicators and graphical outputs can be generated from the stored records according to the selected cities and observation periods. This structure allows users to examine different aspects of urban NO_2 variability without repeating the original satellite extraction or independently reconstructing the city datasets for each analysis.



Fig. 1 Processing architecture linking satellite observations, temporal analysis, spatial database management and web-based visualization.

2.2 City selection and spatial units

A purposive sample of 288 cities was assembled across six inhabited continents to represent contrasting geographical, socioeconomic and atmospheric pollution conditions (Table 1; Fig. 2). Candidate locations were obtained from the SimpleMaps world-cities database (SimpleMaps 2024). The selection included national capitals, previously identified industrial and NO_2 hotspots, major port cities, U.S. state capitals and Augsburg as a local reference city (Krotkov et al. 2016; Fioletov et al. 2025). Duplicate city records were removed during the preparation of the sample. This selection was designed for comparative analysis and does not constitute a statistically representative sample of the global urban population.

Table 1. Composition of the 288-city sample by continent and World Bank national income classification.

Classification	Category	Cities
Continent	Asia	77
	Africa	62
	Europe	57
	North America	56
	South America	22
	Oceania	14
National income	High income	120
	Upper-middle income	73
	Lower-middle income	60
	Low income	29
	Unclassified	6
Total		288

Population and population-density attributes were linked to the city records using ancillary demographic data associated with the United Nations World Urbanization Prospects, while national income classifications were obtained from the World Bank (United Nations 2018; World

Bank 2026). The cities were also divided into three latitude groups: Northern extratropical (greater than 23.5° N), tropical (23.5° S–23.5° N) and Southern extratropical (below 23.5° S). The corresponding groups contained 158, 110 and 20 cities, respectively. Six cities without a World Bank income classification were retained in the geographical and overall analyses but excluded from comparisons between income categories.

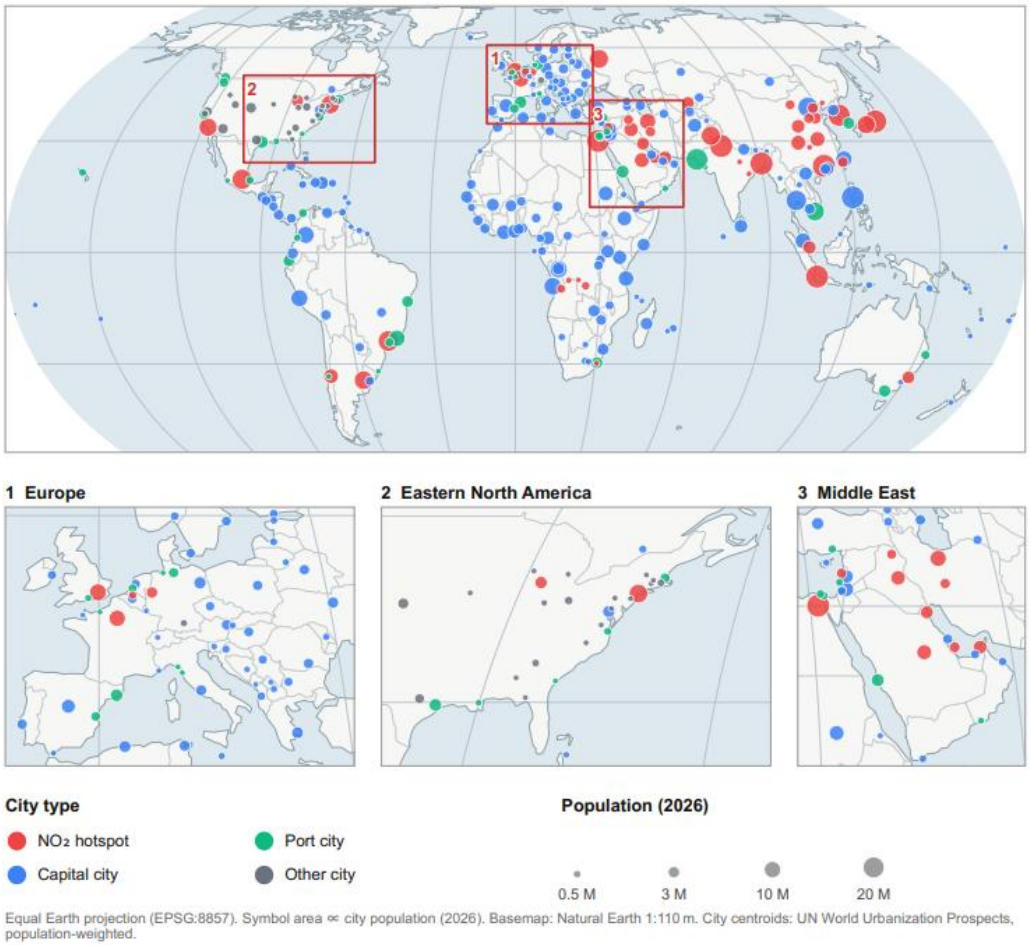


Fig. 2 Geographical distribution of the 288 selected cities. Symbols indicate the stored city categories, while symbol size represents the population attribute used in the original dataset.

Urban footprints were primarily derived from the Global Human Settlement Layer Urban Centre Database (GHS-UCDB R2024A; European Commission, Joint Research Centre 2024). The matching procedure first identified urban-centre polygons intersecting the city reference point. Where no intersection was found, a nearby polygon could be assigned based on an approximate proximity criterion corresponding to a nominal 25-km threshold. In the implemented procedure, proximity was evaluated in geographical coordinates using a fixed degree-to-distance conversion rather than a geodesic calculation.

When no suitable GHSL polygon was identified, a circular buffer with a 20-km radius was generated around the city centroid using a locally estimated UTM projection. Approximately three-quarters of the cities were represented by GHSL urban-centre polygons, while the remainder used these alternative buffers. Both geometry types were stored in PostGIS and used as spatial units to extract satellite observations. Consequently, the resulting city-level NO_2 summaries correspond to the assigned footprints, which do not necessarily coincide with administrative boundaries or the full geographical extent of metropolitan areas.

2.3 Sentinel-5P observations and city-level NO_2 extraction

Tropospheric NO_2 observations were obtained from the Sentinel-5P offline Level-3 collection (COPERNICUS/S5P/OFFL/L3_NO2) available through Google Earth Engine for June 2018–August 2026 (Gorelick et al. 2017; van Geffen et al. 2022; Google Earth Engine 2026). The collection includes retrieval-quality screening applied during the conversion of Sentinel-5P Level-2 products to the gridded Level-3 representation. Additional screening in the present workflow was based on the cloud_fraction band, separately from the quality criteria incorporated in the source collection.

For each city and month, the extraction used the tropospheric_NO2_column_number_density and cloud_fraction bands. Pixels with cloud fractions at or above an initial threshold of 0.20 were excluded. A temporal median of the remaining observations was calculated for each pixel to generate the monthly composite. Spatial median, mean, standard deviation and pixel-count statistics were then calculated within the assigned urban footprint using reduceRegion, with a nominal analysis scale of 5,000 m, bestEffort enabled, and maxPixels set to 10^9.

When the initial threshold did not produce a valid monthly spatial median, the cloud-fraction criterion was progressively relaxed to 0.25, 0.30, 0.35, 0.40, 0.50, 0.60, 0.70, 0.80, 0.90 and 1.00, stopping when a valid result became available. The selected cloud threshold and number of queried satellite images were recorded for each city-month. The image count was obtained before cloud masking and therefore represents the number of queried scenes rather than the number of valid observations contributing to the final composite. Spatial pixel counts were calculated during extraction but were not retained as separate fields in the monthly database model. The resulting NO_2 column values were converted from mol m^{-2} to μmol m^{-2}.

Monthly observations were aggregated into annual and seasonal records. The annual median for each city was calculated as the median of its available monthly spatial medians within the corresponding calendar year. The annual mean was calculated separately as the arithmetic mean of the available monthly spatial means. The number of valid months was retained for each annual

record.

The first and last calendar years were incomplete, covering June–December 2018 and January–August 2026, respectively. The full available series was retained for descriptive analysis, while a separate temporal sensitivity analysis was conducted using the seven complete calendar years from 2019 to 2025.

2.4 Derived indicators and trend classification

Annual changes in urban tropospheric NO_2 were estimated using the Theil–Sen estimator (Sen 1968), while the presence of a monotonic trend was evaluated using the two-sided Mann–Kendall test (Mann 1945; Kendall 1975). Both methods were applied to the annual city-level median series.

For city c, with annual values y observed in year t, the Theil–Sen slope was calculated as the median of all pairwise slopes:

$$\hat{\beta}_c = \mathrm{median}_{1 \le i < j \le n_c} \left(\frac{y_{c,j} - y_{c,i}}{t_j - t_i} \right) \tag{1}$$

The Mann–Kendall statistic was calculated from the signs of pairwise differences between annual observations:

$$S_c = \sum_{i=1}^{n_c - 1} \sum_{j=i+1}^{n_c} \mathrm{sgn}\left(y_{c,j} - y_{c,i}\right) \tag{2}$$

The corresponding standardized statistic was obtained using a continuity correction:

$$Z_c = \begin{cases} \dfrac{S_c - 1}{\sqrt{\mathrm{Var}(S_c)}} & S_c > 0, \\ 0 & S_c = 0, \\ \dfrac{S_c + 1}{\sqrt{\mathrm{Var}(S_c)}} & S_c < 0. \end{cases} \tag{3}$$

The null variance accounts for tied annual values:

$$\mathrm{Var}(S_c) = \frac{n_c(n_c - 1)(2n_c + 5) - \sum_g u_g \left(u_g - 1\right)\left(2u_g + 5\right)}{18} \tag{4}$$

Here, $n_{(c)}$ is the number of annual observations for city c, and $u_{(g)}$ is the number of observations in tie group g. Two-sided p-values were calculated using the normal approximation. Cities with positive or negative slopes and unadjusted p-values of 0.05 or less were classified as nominal

increases or decreases, respectively. All other cities were classified as having no nominal trend detection. Slope estimates were retained regardless of statistical classification.

Because trend testing was conducted for 288 cities, the Benjamini–Hochberg false-discovery-rate procedure was used to account for multiple comparisons (Benjamini and Hochberg 1995). For the ordered p-values, the adjusted values were calculated as:

$$q_{(j)} = \min_{k \geq j} \left\{ \min \left(1, \frac{m}{k} p_{(k)} \right) \right\}, \qquad m = 288. \tag{5}$$

In Eq. (5), $p_{(k)}$ denotes the kth ordered p-value, $q_{(j)}$ its monotone-adjusted value and m the total number of tests. The adjustment was applied to the four-decimal p-values available in the exported city results. Nominal classifications and multiplicity-adjusted results were reported separately, with individual city statistics provided in Supplementary Material, Tables S1 and S3.

Trend calculations were implemented in Python using pairwise slope estimation and pyMannKendall (Hussain and Mahmud 2019), with a SciPy Kendall-tau implementation available as a fallback (Virtanen et al. 2020). Given the short annual record, the trend tests were treated as exploratory indicators of the direction and consistency of observed changes.

Temporal sensitivity was assessed by repeating the trend analysis for the seven complete calendar years 2019–2025. The results were compared with those from the full available period, which included the incomplete boundary years 2018 and 2026.

Additional indicators were used to describe temporal variability. The long-term city-level NO_2 value was defined as the arithmetic mean of annual median values, assigning equal weight to each available year. Monthly climatologies were calculated from the available observations for each calendar month.

Seasonal amplitude was calculated from the stored seasonal records as the difference between the highest and lowest climatological seasonal values for each city. Winter–summer contrasts were calculated as December–February minus June–August for Northern extratropical cities and the reverse for Southern extratropical cities. For tropical cities, stored seasonal records distinguish June–September from October–May, whereas a separate seasonal contrast compares June–September with November–April. These fixed calendar groupings were not derived from local rainfall seasons.

The 2020 anomaly was calculated as the percentage difference between the 2020 and 2019 annual median NO_2 values. Potential changes in the annual series were also examined using the Pettitt test (Pettitt 1979). Given the limited number of annual observations, this test was considered descriptive rather than definitive evidence for the presence or absence of persistent structural

change.

2.5 Exploratory city groupings

Exploratory grouping of urban NO_2 behaviour was performed using k-means clustering based on four descriptors: (i) the arithmetic mean of annual city-level median NO_2 values, (ii) the annual Theil–Sen slope, (iii) seasonal amplitude, and (iv) the variance of the monthly city-median series. The fourth descriptor represents the variability of available monthly observations and was calculated without removing the seasonal cycle.

The four variables were standardized to zero mean and unit variance using StandardScaler to prevent differences in measurement units and numerical ranges from directly determining the clustering. K-means was then applied using Euclidean distances, ten initializations and a fixed random seed of 42. Candidate solutions containing four, five and six groups were compared using the silhouette coefficient (Rousseeuw 1987).

Principal component analysis was used to visualize the resulting groups in a two-dimensional feature space. Ward hierarchical clustering was also examined as an alternative grouping approach (Ward 1963; Pedregosa et al. 2011). The resulting groups were treated as descriptive summaries of similarities among the four input features rather than predefined atmospheric regimes.

For additional geographical comparisons, long-term NO_2 levels, annual slopes and nominal trend classifications were summarized by continent and World Bank national income group. These comparisons were descriptive and did not account for meteorological differences, emission inventories, or other potential confounding variables.

2.6 Database implementation and interactive analysis

The spatial database was implemented in PostgreSQL/PostGIS and organized around a City model linked to three observation tables: NO2Monthly, NO2Annual and NO2Seasonal. The City model stores geographical attributes, the reference point and alternative urban geometries using the EPSG:4326 coordinate reference system. Foreign-key relationships connect the observation records to a unique city identifier, while unique city–time combinations distinguish monthly, annual and seasonal observations.

The monthly table retains the principal NO_2 summary statistics, the number of queried images and the effective cloud-fraction threshold. The annual and seasonal tables store the corresponding temporal summaries and observation counts. These records provide the basis for the statistical

277 analysis without requiring the repeated retrieval of satellite observations.

278 The Django/GeoDjango application accesses the database through a Python service layer and
279 JSON-based interfaces. Statistical summaries, trend indicators, and exploratory groupings are
280 calculated from stored observations for user-selected cities, periods, and contextual categories.
281 The application provides ten visualization families and twelve predefined configurations,
282 including geographical distributions, temporal trajectories, seasonal profiles and comparisons by
283 continent, latitude group, city type, population, population density and national income
284 classification.

285 Results can be exported as CSV tables and PNG figures. For example, a user can select a group
286 of cities, examine their long-term NO_2 columns, compare their estimated annual slopes and
287 inspect their seasonal profiles while retaining the same city definitions throughout the analysis.
288 The system therefore connects spatial identities, satellite-derived observations and temporal
289 indicators within a common environment for comparative urban NO_2 analysis.

290

291 **3. Results**

292 **3.1 Integrated geospatial outputs and urban NO_2 distribution**

293 The web application developed for this study is accessible at https://no2.aruns.de/. It links city
294 geometries and contextual attributes to monthly, annual and seasonal NO_2 observations through
295 a persistent city identifier. For the 288-city sample, users can examine geographical distributions,
296 annual trajectories, estimated trends and seasonal profiles using consistent city selections across
297 analytical views. The interface provides ten visualization families and twelve predefined
298 configurations, with filters for cities, time periods and contextual attributes. Maps, graphical
299 results and numerical tables can be exported without repeating the original Sentinel-5P extraction.
300 Figure 3 presents the map and analytical interfaces, and Supplementary Material, Fig. S1 shows
301 ranked-city and time-series views. The live application is updated independently of the
302 manuscript analysis, which uses observations through August 2026. Software response times and
303 external usability were not independently evaluated. The city-level results used below are
304 provided in Supplementary Material, Table S1.

305 Long-term city mean tropospheric NO_2 columns ranged from 2.77 μmol m^{-2} in South Tarawa to
306 386.22 μmol m^{-2} in Tehran. The cross-city median was 37.79 μmol m^{-2} (interquartile range,
307 22.26–59.45 μmol m^{-2}), whereas the arithmetic mean was 49.56 μmol m^{-2}. The next-highest cities
308 after Tehran were Beirut (201.62 μmol m^{-2}), Baghdad (186.06), Tashkent (173.81), and Dubai
309 (170.85). At the lower end, Port Vila, Suva and Apia each had a long-term city mean below 6
310 μmol m^{-2}. The full ranked distribution is provided in the Supplementary Material, Fig. S2; the

geographical locations of all sampled cities are shown in Fig. 2.

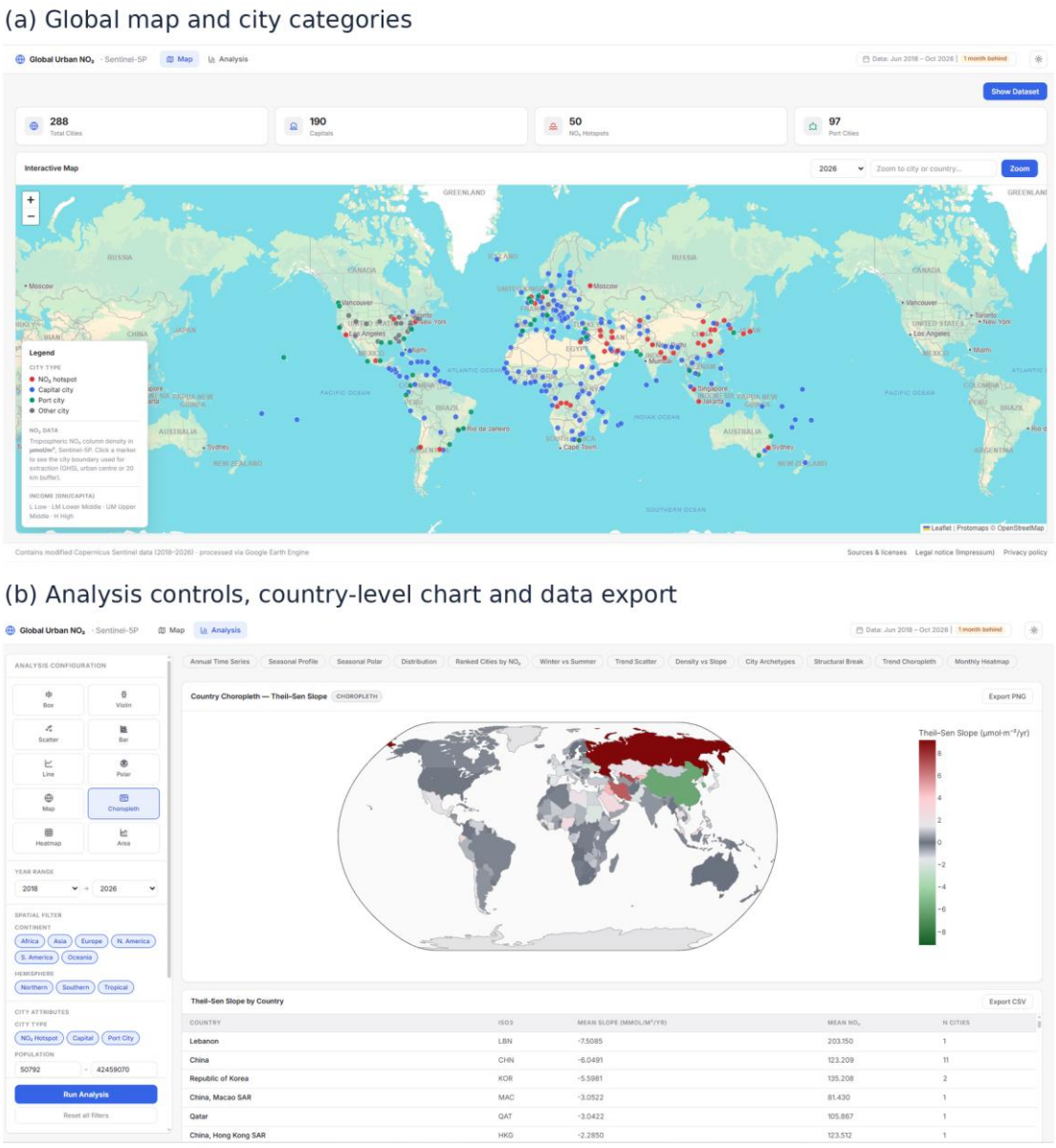


Fig. 3 Web application interfaces: (a) interactive map of the 288 selected cities and their stored categories; (b) analytical view with geographical filters, country-level summaries of the included sample cities and CSV/PNG export controls. Screenshots supplied by the authors on 23 November 2026. The live application displayed records through October 2026, whereas the statistical results in this manuscript use observations through August 2026; values displayed in the live interface are not necessarily identical to the frozen analysis outputs.

3.2 Annual trend estimates, multiple testing and temporal sensitivity

Across the 288 annual city-median series, 157 Theil–Sen slopes were positive and 131 were negative. The median slope was +0.047 µmol m^{-2} yr^{-1} (interquartile range, −0.439 to +0.545 µmol m^{-2} yr^{-1}). Individual estimates ranged from −12.825 µmol m^{-2} yr^{-1} in Handan to +9.537 µmol m^{-2}

yr^{-1} in Tehran (Figs. 4 and 5). Jinan (−11.938) and Xi'an (−9.196) also had large negative slopes, while Moscow (+9.260), Riyadh (+6.679) and Baghdad (+5.947) had large positive slopes. Tehran had an unadjusted Mann–Kendall p-value of 0.7545 despite its large positive slope (Supplementary Material, Table S1).

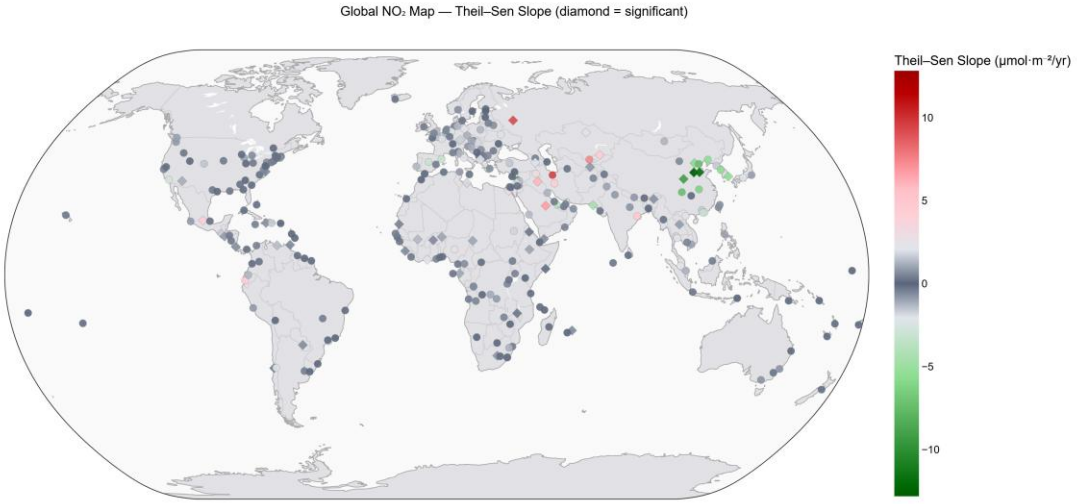


Fig. 4 Geographical distribution of city-level Theil–Sen slopes from annual NO_2 median series (2018–2026). Diamond symbols indicate nominal Mann–Kendall detections at unadjusted $p \leq 0.05$; no city passed the 5% FDR threshold.

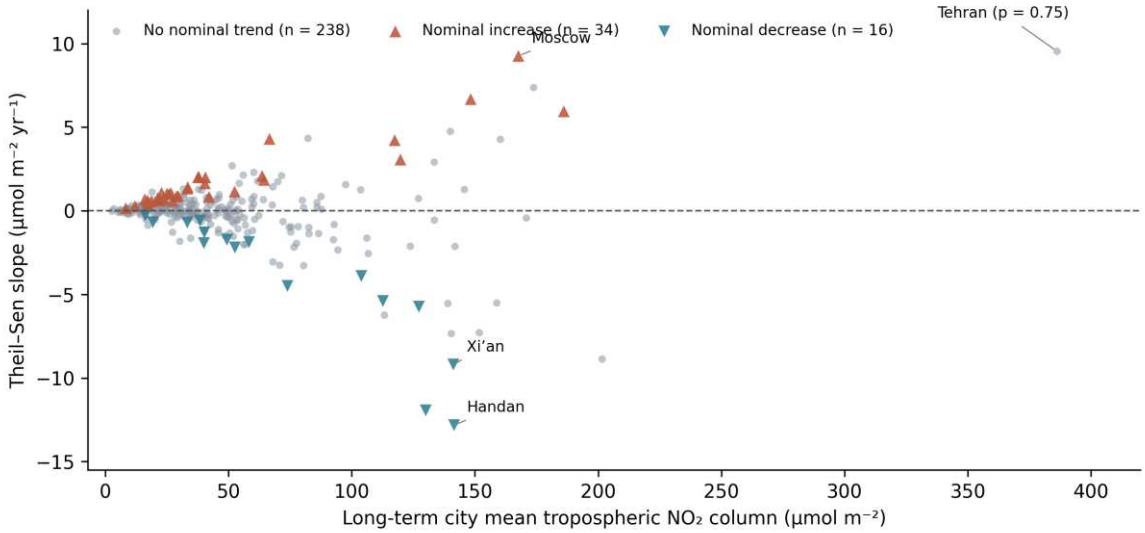


Fig. 5 Relationship between the long-term mean NO_2 column and the Theil–Sen slope for 288 cities. Symbols reflect unadjusted trend classifications. The Tehran value is shown separately as an extreme-level city.

Using the nominal Mann–Kendall threshold of $p \leq 0.05$, 34 cities were classified as increasing and 16 as decreasing; the remaining 238 had no nominal detection. After Benjamini–Hochberg adjustment across 288 city-level tests, no trend met the false-discovery-rate threshold of 0.05 (minimum adjusted

q = 0.1568; Supplementary Material, Table S3).

When the analysis was repeated for the seven complete calendar years 2019–2025, the number of nominal detections was 19 increases and four decreases, compared with 34 and 16 for June 2018–August 2026 (Fig. 6).

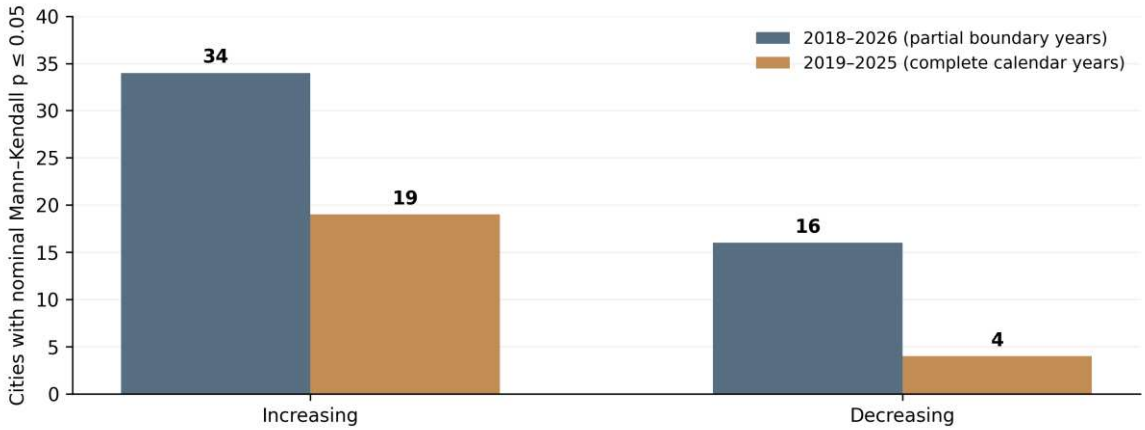


Fig. 6. Comparison of nominal increasing- and decreasing-trend detections for the complete available interval (2018–2026) and the complete calendar-year interval (2019–2025).

3.3 Contrasts by continent and national income group

Long-term NO_2 levels differed among the sampled geographical regions (Table 2). Asia had the highest median city mean (67.78 µmol m^{-2}), followed by Europe (46.00), North America (35.51), South America (26.12), Africa (21.11) and Oceania (9.01). By World Bank national income classification, median city means were 45.96 µmol m^{-2} for the high-income group, 40.45 for upper-middle-income, 30.64 for lower-middle-income and 19.80 for low-income cities. Six unclassified cities contributed to the overall and continent summaries but not the four-category income comparison.

The median annual slope was negative among high-income cities (−0.20 µmol m^{-2} yr^{-1}) and positive among upper-middle-income (+0.10), lower-middle-income (+0.25) and low-income cities (+0.28; Table 2, Fig. 7). In the four income groups, positive estimated slopes occurred in 42 of 120, 44 of 73, 47 of 60 and 21 of 29 cities, respectively. The corresponding counts of nominally detected increases were four, 15, seven and eight. At continental scale, Europe had a median slope of −0.39 µmol m^{-2} yr^{-1} (50 of 57 city slopes negative), whereas Africa had a median slope of +0.23 (50 of 62 positive). Asia included both positive and negative estimates, with eight

nominal increases and nine nominal decreases.

Table 2 Long-term median city means and annual Theil–Sen slopes by income group and continent. Nominal increase/decrease counts use unadjusted Mann–Kendall $p \leq 0.05$; no city passed FDR correction. NO_2 in µmol m^{-2}, slopes in µmol m^{-2} yr^{-1}.

Group	n	Median NO_2	Median slope	Nominal ↑	Nominal ↓
A. World Bank national income group					
High income	120	46.0	−0.20	4	8
Upper-middle income	73	40.5	+0.10	15	4
Lower-middle income	60	30.6	+0.25	7	2
Low income	29	19.8	+0.28	8	2
Unclassified	6	9.7	+0.02	0	0
B. Continent					
Africa	62	21.1	+0.23	15	1
Asia	77	67.8	+0.27	8	9
Europe	57	46.0	−0.39	2	4
North America	56	35.5	+0.08	6	2
South America	22	26.1	+0.07	3	0
Oceania	14	9.0	−0.05	0	0

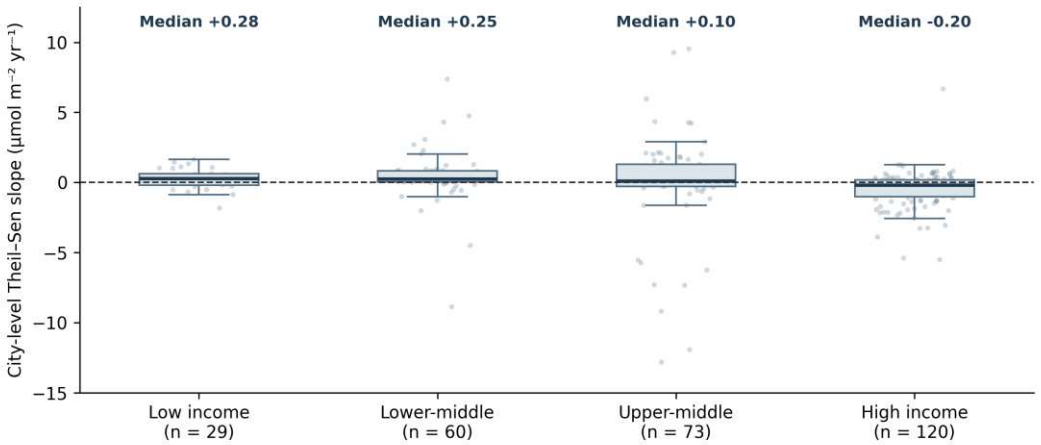


Fig. 7 Distributions of city-level Theil–Sen slopes by World Bank national income group (n = 282 classified cities). Horizontal reference line indicates zero slope; labels report group medians.

3.4 Seasonal variation and exploratory urban NO_2 groups

The median city-level seasonal amplitude was 18.7 µmol m^{-2}. It was approximately 31 µmol m^{-2} for Northern extratropical cities (n = 158) and 18 µmol m^{-2} for Southern extratropical cities (n = 20), compared with 4.9 µmol m^{-2} for tropical cities (n = 110). The hemisphere-adjusted winter-

minus-summer contrast was positive for most extratropical cities, with a median of approximately +29 µmol m⁻². The aggregated monthly profiles showed higher NO_2 columns during December–February north of 23.5° N and during June–August south of 23.5° S (Fig. 8).

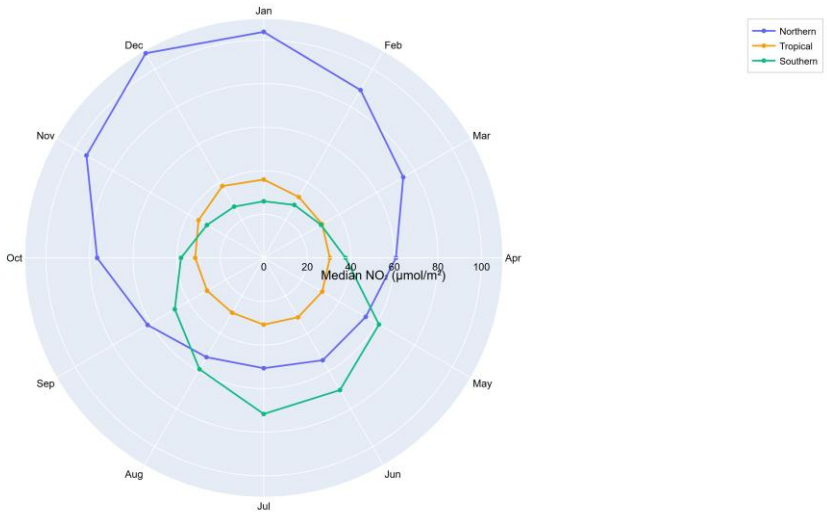


Fig. 8 Monthly NO_2 climatological profiles for Northern extratropical (n = 158), tropical (n = 110) and Southern extratropical (n = 20) city groups.

Clustering the four standardized descriptors (long-term column, annual slope, seasonal amplitude and monthly variance) produced a four-group partition with the largest silhouette coefficient among the tested candidate solutions (approximately 0.68). The groups contained 1, 16, 15 and 256 cities, respectively (Fig. 9). Tehran formed a singleton group with a mean column of 386.2 µmol m⁻² and slope of +9.54 µmol m⁻² yr⁻¹. Two small high-column groups had similar mean levels (135.7 and 132.3 µmol m⁻²) but opposite mean slopes (+3.73 and −6.60 µmol m⁻² yr⁻¹). The remaining 256 cities had a mean column of 38.0 µmol m⁻² and a mean slope close to zero, although this group included at least 18 cities with nominal trend detections. It was therefore not treated as a group of statistically stable cities (Table 3).

Table 3 Descriptive NO_2 levels and annual slopes of the four exploratory k-means groups; the partition uses four standardized features. Group means are in µmol m⁻² and µmol m⁻² yr⁻¹.

Group	Description	n	Mean NO_2	Mean slope
1	Tehran singleton	1	386.2	+9.54
2	High-column, positive mean slope	16	135.7	+3.73
3	High-column, negative mean slope	15	132.3	−6.60
4	Lower-column, heterogeneous	256	38.0	0.00

The six-group sensitivity partition returned a lower silhouette coefficient (0.45; Supplementary

Material, Fig. S3). A Ward hierarchical grouping is presented in Supplementary Material, Fig. S4.

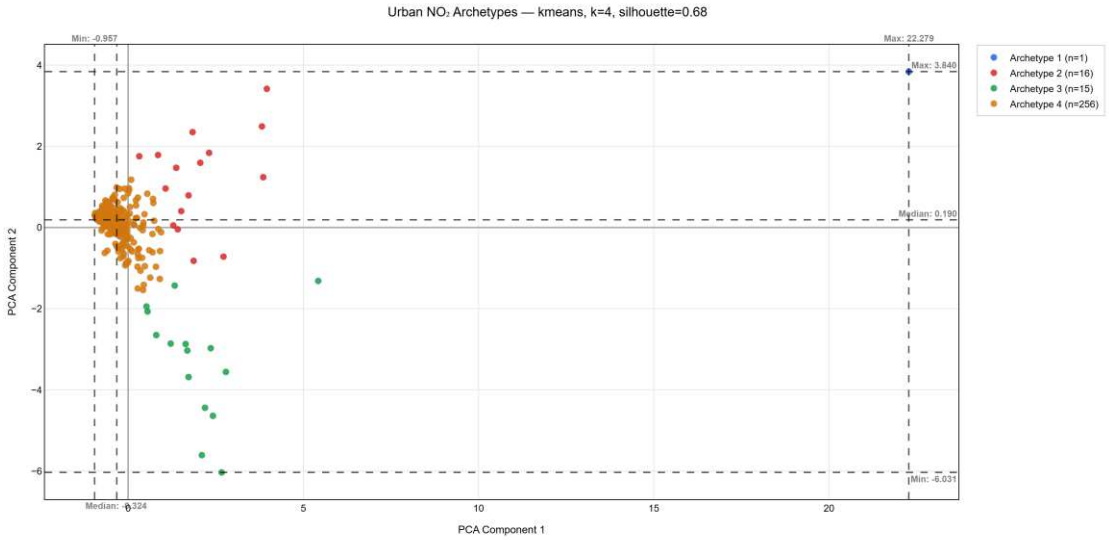


Fig. 9 Two-component principal-component projection of k-means groups based on long-term NO_2 level, annual slope, seasonal amplitude and monthly variance. The Tehran singleton is separated from the multi-city groups.

3.5 The 2020 anomaly and aggregation sensitivity

The annual city-level NO_2 median was lower in 2020 than in 2019 for 225 of the 288 selected cities (78.1%). The median relative difference across cities was −8.1%, with continental median anomalies ranging from −11.5% in Oceania and −10.7% in Europe to −2.3% in Africa (Table 4). The interannual comparison was not adjusted for changes in atmospheric conditions or emissions, and the observed difference is reported without causal attribution.

For the annual Pettitt diagnostic, reported nominal p-values were approximately 0.10 or greater (median $p \approx 0.69$). No change-point interpretation was based on this test, given the limited annual series. The 2021 split sensitivity plot is retained in Supplementary Material, Fig. S5. Separately, the comparison of mean- and median-based city summaries had a median signed relative difference of +7.8% (interquartile range, +3.0% to +12.0%; Supplementary Material, Table S2).

Table 4 Median relative difference in annual city-level NO_2 medians between 2020 and 2019. Negative values denote lower annual NO_2 in 2020.

Continent	Cities (n)	Median 2020 anomaly (%)
Africa	62	−2.3
Asia	77	−8.5
Europe	57	−10.7
North America	56	−10.1

Continent	Cities (n)	Median 2020 anomaly (%)
Oceania	14	−11.5
South America	22	−8.2
All cities	288	−8.1

4. Discussion

4.1 Integrating Earth Observation data for comparative urban analysis

The main contribution of this study is the integration of satellite observations, urban spatial units and temporal indicators within a common geospatial information system. The implemented platform connects city geometries and contextual attributes with monthly, annual and seasonal NO_2 records through persistent identifiers, allowing the same cities to be examined using different analytical approaches. Through the web application (https://no2.aruns.de/), users can compare geographical distributions, estimated trends and seasonal profiles while maintaining consistent spatial references and observation periods. This approach separates satellite extraction from subsequent analysis and visualization, supporting repeated comparisons without reprocessing the original imagery.

Previous applications have demonstrated the potential of Google Earth Engine and web-based interfaces for exploring satellite-derived air pollution information (Alvarez-Mendoza et al. 2023; Shikwambana et al. 2025). The present study builds on these developments by organizing observations and analytical indicators within a relational spatial database rather than treating each visualization as a separate processing task. Its contribution is therefore not a new retrieval method or visualization algorithm, but the connection between spatial data management and comparative analysis. This is consistent with broader efforts to improve the accessibility, organization and reuse of Earth Observation datasets (Mahecha et al. 2020; Wilkinson et al. 2016; Scheick et al. 2026). The resulting application provides a practical example of how different geospatial technologies can be combined to examine environmental observations across geographical and temporal scales.

A further advantage of this structure is the possibility of comparing cities through several indicators without assuming that a single statistic adequately describes their atmospheric conditions. For example, cities with similar long-term NO_2 columns can be examined according to their estimated annual changes or seasonal characteristics. Maintaining these indicators within a common system also provides a basis for identifying locations that warrant more detailed environmental investigation, particularly where conventional monitoring networks are limited. Such comparisons offer an initial screening perspective rather than a direct assessment of surface pollution, population exposure or the urgency of intervention.

4.2 What combined NO_2 indicators reveal across cities

The results show the differences between absolute atmospheric NO_2 levels and their temporal behaviour. Although the selected high-income cities generally exhibited higher long-term columns, their median estimated slope was slightly negative, whereas the lower-income categories showed positive median slopes. Similar geographical differences were observed between continents, including negative median slopes among European cities and contrasting trajectories across parts of Asia and Africa. Previous satellite studies have documented changes in established industrial regions and emerging urban hotspots (Geddes et al. 2016; Krotkov et al. 2016; Fioletov et al. 2025). More recent analyses have examined urban scaling, global changes across thousands of cities and trends adjusted for meteorological variability (Wurm et al. 2025; Huber et al. 2026; Hassani et al. 2026). The patterns observed here are broadly comparable with these investigations, although the present sample and analytical procedures do not support direct estimates of global urban trends.

An important distinction concerns the magnitude of estimated slopes and the statistical evidence supporting them. Of the 288 cities, 50 showed nominal Mann–Kendall detections, but none remained significant after false-discovery-rate correction. Furthermore, restricting the analysis to the complete calendar years 2019–2025 reduced the number of nominal detections to 23. These findings indicate that trend classifications depend on the temporal window and the statistical criterion applied. The decrease in detections cannot be attributed solely to the removal of incomplete years because the sensitivity analysis also reduces the number of annual observations. Consequently, estimated slopes are useful descriptive indicators, but they should not be interpreted as confirmed changes in atmospheric pollution for individual cities.

The exploratory city groupings provide another example of why multiple indicators are useful. Two groups had comparable mean NO_2 columns but opposite mean annual slopes, distinguishing cities with similar atmospheric levels but different estimated trajectories. However, the clustering was strongly affected by the extreme values associated with Tehran, which formed a separate group, while most cities were assigned to a broad and heterogeneous lower-column group. These results support the use of clustering as an exploratory comparison of atmospheric characteristics rather than as evidence of distinct or stable pollution regimes. Seasonal analysis provided additional differentiation, with stronger winter–summer contrasts in the extratropics and relatively smaller amplitudes in tropical cities. Such differences are consistent with variations in atmospheric chemistry, boundary-layer conditions and seasonal emissions, although these processes were not explicitly evaluated in the present analysis.

The widespread negative NO_2 anomaly observed in 2020 also shows the importance of temporal context. Earlier studies documented substantial reductions in atmospheric NO_2 during COVID-19

restrictions (Bauwens et al. 2020; Cooper et al. 2022). In the present sample, the median 2020 anomaly relative to 2019 was −8.1%, with negative differences in approximately 78% of cities. Nevertheless, the annual comparison does not separate changes in anthropogenic emissions from meteorological variability or other influences. The short annual record also limits the interpretation of change-point tests, which cannot provide reliable evidence of persistent structural changes in this setting. These results reinforce the importance of examining temporal coverage and analytical uncertainty alongside the observed differences.

4.3 Interpretation, applicability and future developments

The integration of satellite observations, spatial databases and temporal indicators provides opportunities for comparing atmospheric conditions across cities with different geographical and socioeconomic characteristics. An important aspect of this approach is the use of a common source of Earth Observation data, particularly in regions where ground-based air-quality monitoring is limited or unavailable. Although Sentinel-5P measures tropospheric NO_2 columns rather than surface concentrations, these observations provide complementary information for examining spatial differences and temporal variability. Their relationship with ground-level pollution depends on atmospheric transport, chemical processes and meteorological conditions. Recent studies have demonstrated how satellite information can be combined with additional environmental predictors to estimate surface NO_2 and $PM_{2.5}$ concentrations (Miller et al. 2026). The present platform focuses instead on the consistent organization and comparison of satellite-derived observations, providing a basis for future integration with surface measurements and atmospheric models.

The geographical diversity of the selected cities shows both the applicability of the workflow and the importance of maintaining consistent spatial definitions. Urban areas differ in population, geographical extent, land-use characteristics and surrounding environments, making direct comparisons challenging. The study addresses this through a common satellite-processing procedure and the preferential use of GHSL urban-centre polygons, complemented by 20-km buffers where suitable polygons were unavailable. While this approach allows the selected cities to be included within the same analytical structure, differences between spatial footprints and the purposive selection of cities should be considered when interpreting geographical patterns.

Temporal analysis further demonstrates the value of preserving observation periods alongside statistical indicators. The differences between the full observation window and the complete-year analysis show how estimated trends and their statistical classifications can change with temporal coverage. Although the city-level slopes provide useful information about the direction and magnitude of observed variability, none remained significant after correction for multiple testing.

In addition, meteorological conditions were not explicitly normalized, so the observed changes cannot be attributed directly to emission policies or particular economic activities. By retaining the underlying temporal records, the platform allows these indicators to be examined alongside their observation periods instead of presenting a single trend classification as a definitive description of urban atmospheric change.

From an informatics perspective, the implemented system demonstrates how satellite extraction, persistent spatial identifiers, relational data storage and interactive analytical outputs can be connected within a common workflow. Its current implementation supports comparisons among cities, observation periods and geographical categories without repeating satellite extraction. Independent deployment, processing performance and user experience remain areas for future evaluation, while a documented software release would facilitate reproducibility and reuse beyond the current application.

Further development could incorporate ground-based air-quality measurements, meteorological information, additional atmospheric products and more detailed observation-quality indicators. These extensions would support more comprehensive environmental assessments while retaining the existing relationships between urban spatial units and temporal observations. In this way, the platform provides a starting point for expanding comparative Earth Observation analysis and making environmental information more accessible to researchers and institutions working across different monitoring contexts.

5. Conclusion

This study developed a web-based geospatial platform integrating Sentinel-5P observations, urban spatial data and temporal indicators to support comparative analysis of atmospheric NO_2. The implementation connects satellite-derived observations with persistent city geometries and contextual information through a PostgreSQL/PostGIS database, allowing geographical distributions, annual trends and seasonal variability to be examined within a common analytical environment. Its application to 288 cities shows how different geospatial technologies can be combined to organize and explore Earth Observation data without repeatedly processing the original satellite imagery.

The results showed substantial geographical differences in tropospheric NO_2 columns, with a median long-term value of 37.8 μmol m^{-2} across the selected cities. Estimated annual slopes and seasonal profiles varied between cities and geographical regions, showing how temporal indicators provide additional information beyond absolute NO_2 levels. Although 50 cities showed nominal trend detections, none remained significant after correction for multiple comparisons,

and the number of detections decreased when the analysis was restricted to complete calendar years. These findings highlight the importance of considering temporal coverage and statistical uncertainty when interpreting satellite-derived urban pollution indicators.

Beyond the atmospheric findings, the study shows the value of linking satellite observations, spatial databases and interactive analytical tools for examining environmental conditions across cities with different monitoring contexts. The platform provides a common basis for comparing available observations and identifying patterns that may warrant further investigation, particularly in regions with limited ground-based monitoring. Future integration of surface measurements, meteorological information and additional Earth Observation products could extend its analytical capabilities and support more comprehensive urban environmental assessments.

Acknowledgements

The authors acknowledge the European Space Agency, the Copernicus programme, the European Commission Joint Research Centre, Google Earth Engine, the World Bank, and the United Nations for providing the open datasets used in this study. The authors also thank colleagues at the University of Augsburg and the German Aerospace Center for scientific discussion.

Statements and Declarations

Data and code availability

City-level results, comparisons of mean- and median-based summaries, multiple-testing results and additional figures are provided in the Supplementary Material and accompanying CSV files. Sentinel-5P Level-3 observations and GHSL urban boundaries are available from their respective public providers. The application is accessible at https://no2.aruns.de/ and may display observations more recent than the August 2026 endpoint used in the manuscript analyses. The implementation code and processing configurations have not been deposited in a versioned public repository; requests for access can be directed to the corresponding author.

Competing interests

The authors declare that they have no competing interests.

Funding

This research received no specific grant from any funding agency in the public, commercial, or not-for-profit sectors.

Author contributions

J.O.: data curation, software development, formal analysis, visualization, and preparation of the

initial manuscript draft. M.W.: interpretation of Earth Observation and urban results, critical revision of the manuscript. C.I.A.: conceptualization, supervision, methodology, interpretation of results, manuscript development and revision. All authors reviewed and approved the final manuscript.

Declaration of generative AI and AI-assisted technologies in the writing process

During the preparation of this manuscript, the authors used ChatGPT 6.0 (OpenAI) and Grammarly for language editing and improving readability. The authors reviewed the final content and take full responsibility for the manuscript.

References

Alvarez CI, Schneider P, Wurm M, Knote C (2026) Urban–background gradients reveal contrasting satellite-derived NO_2 pollution regimes across Latin American cities. Atmospheric Pollution Research 17:103265. https://doi.org/10.1016/j.apr.2026.103265

Alvarez-Mendoza CI, Teodoro AC, Torres N, Vivanco V (2019) Assessment of remote sensing data to model PM10 estimation in cities with a low number of air quality stations: A case of study in Quito, Ecuador. Environments 6(7):85. https://doi.org/10.3390/environments6070085

Alvarez-Mendoza CI, Vasquez D, Lopez S (2023) Monitoring air quality using remote sensing based on a Google Earth Engine application in countries with limited air quality data and control policies: A case study in Ecuador. In Remote Sensing Technologies and Applications in Urban Environments VIII (Proceedings of SPIE, Vol. 12735, Article 127350B). https://doi.org/10.1117/12.2672325

Bauwens M, Compernolle S, Stavrakou T, Müller J-F, van Gent J, Eskes H, Levelt PF, van der A R, Veefkind JP, Vlietinck J, Yu H, Zehner C (2020) Impact of coronavirus outbreak on NO_2 pollution assessed using TROPOMI and OMI observations. Geophysical Research Letters 47(11):e2020GL087978. https://doi.org/10.1029/2020GL087978

Benjamini Y, Hochberg Y (1995) Controlling the false discovery rate: A practical and powerful approach to multiple testing. Journal of the Royal Statistical Society: Series B 57(1):289–300. https://doi.org/10.1111/j.2517-6161.1995.tb02031.x

Cooper MJ, Martin RV, Hammer MS, Levelt PF, Veefkind P, Lamsal LN, Krotkov NA, Brook JR, McLinden CA (2022) Global fine-scale changes in ambient NO_2 during COVID-19 lockdowns. Nature 601:380–387. https://doi.org/10.1038/s41586-021-04229-0

European Commission, Joint Research Centre (2024) GHS Urban Centre Database R2024A (GHS-UCDB) [Dataset]. European Commission. https://doi.org/10.2905/JRC.05RDPR0

Fioletov V, McLinden CA, Griffin D, Zhao X, Eskes H (2025) Global seasonal urban, industrial, and background NO_2 estimated from TROPOMI satellite observations. Atmospheric Chemistry and

Physics 25:575–596. https://doi.org/10.5194/acp-25-575-2025

Geddes JA, Martin RV, Boys BL, van Donkelaar A (2016) Long-term trends worldwide in ambient NO_2 concentrations inferred from satellite observations. Environmental Health Perspectives 124(3):281–289. https://doi.org/10.1289/ehp.1409567

Google Earth Engine (2026) COPERNICUS/S5P/OFFL/L3_NO2: Sentinel-5P OFFL NO_2: Offline nitrogen dioxide. Earth Engine Data Catalog. https://developers.google.com/earth-engine/datasets/catalog/COPERNICUS_S5P_OFFL_L3_NO2

Gorelick N, Hancher M, Dixon M, Ilyushchenko S, Thau D, Moore R (2017) Google Earth Engine: Planetary-scale geospatial analysis for everyone. Remote Sensing of Environment 202:18–27. https://doi.org/10.1016/j.rse.2017.06.031

Hassani A, Walker S-E, Stebel K, Schneider P (2026) Tracking the path to cleaner cities using global urban NO_2 monitoring from space. Environmental Research Letters 21(9):094004. https://doi.org/10.1088/1748-9326/ae5e97

Huber DE, Kerr GH, Nawaz MO, Runkel S, Anenberg SC, Goldberg DL (2026) Global NO_2 changes between 2019 and 2024 as observed by TROPOMI in urban areas and emerging hotspots. Atmospheric Chemistry and Physics 26:3783–3803. https://doi.org/10.5194/acp-26-3783-2026

Hussain MM, Mahmud I (2019) pyMannKendall: A Python package for non parametric Mann Kendall family of trend tests. Journal of Open Source Software 4(39):1556. https://doi.org/10.21105/joss.01556

Kendall MG (1975) Rank correlation methods (4th ed.). Charles Griffin.

Krotkov NA, McLinden CA, Li C, Lamsal LN, Celarier EA, Marchenko SV, et al (2016) Aura OMI observations of regional SO_2 and NO_2 pollution changes from 2005 to 2015. Atmospheric Chemistry and Physics 16:4605–4629. https://doi.org/10.5194/acp-16-4605-2016

Mahecha MD, Gans F, Brandt G, Christiansen R, Cornell SE, Fomferra N, et al (2020) Earth system data cubes unravel global multivariate dynamics. Earth System Dynamics 11(1):201–234. https://doi.org/10.5194/esd-11-201-2020

Mann HB (1945) Nonparametric tests against trend. Econometrica 13(3):245–259. https://doi.org/10.2307/1907187

Miller R, Olbrich J, Wierer M, Chen J, Wurm M, Alvarez CI (2026) Satellite-driven modelling of NO_2 and $PM_{2.5}$ across Germany (2019–2024): A multi-sensor machine-learning approach. Environmental Pollution 396:127898. https://doi.org/10.1016/j.envpol.2026.127898

Pedregosa F, Varoquaux G, Gramfort A, Michel V, Thirion B, Grisel O, et al (2011) Scikit-learn: Machine learning in Python. Journal of Machine Learning Research 12:2825–2830. https://jmlr.org/papers/v12/pedregosa11a.html

Pettitt AN (1979) A non-parametric approach to the change-point problem. Applied Statistics 28(2):126–135. https://doi.org/10.2307/2346729

Rousseeuw PJ (1987) Silhouettes: A graphical aid to the interpretation and validation of cluster analysis. Journal of Computational and Applied Mathematics 20:53–65. https://doi.org/10.1016/0377-0427(87)90125-7

Scheick J, Barrett AP, Fair Z, Katz Z, Lopez L, Neeley A, et al (2026) Ten rules to increase the usability of earth observation mission datasets. Earth Science Informatics, 19, Article 186. https://doi.org/10.1007/s12145-026-02216-5

Sen PK (1968) Estimates of the regression coefficient based on Kendall's tau. Journal of the American Statistical Association 63(324):1379–1389. https://doi.org/10.1080/01621459.1968.10480934

Shikwambana L, Kganyago M, Mbatha N, Mhangara P (2025) Development of an air quality dashboard using Sentinel-5P data. In Remote Sensing of Clouds and the Atmosphere XXX (Proceedings of SPIE, Vol. 13668, Article 136680I). https://doi.org/10.1117/12.3068951

SimpleMaps (2024) World Cities Database. https://simplemaps.com/data/world-cities

United Nations, Department of Economic and Social Affairs, Population Division (2018) World Urbanization Prospects: The 2018 Revision. United Nations. https://population.un.org/wup/

van Geffen J, Eskes H, Compernolle S, Pinardi G, Verhoelst T, Lambert J-C, et al (2022) Sentinel-5P TROPOMI NO_2 retrieval: Impact of version v2.2 improvements and comparisons with OMI and ground-based data. Atmospheric Measurement Techniques 15:2037–2060. https://doi.org/10.5194/amt-15-2037-2022

Veefkind JP, Aben I, McMullan K, Förster H, de Vries J, Otter G, et al (2012) TROPOMI on the ESA Sentinel-5 Precursor: A GMES mission for global observations of the atmospheric composition for climate, air quality and ozone layer applications. Remote Sensing of Environment 120:70–83. https://doi.org/10.1016/j.rse.2011.09.027

Verhoelst T, Compernolle S, Pinardi G, Lambert J-C, Eskes HJ, et al (2021) Ground-based validation of the Copernicus Sentinel-5P TROPOMI NO_2 measurements with the NDACC ZSL-DOAS, MAX-DOAS and Pandonia global networks. Atmospheric Measurement Techniques 14:481–510. https://doi.org/10.5194/amt-14-481-2021

Virtanen P, Gommers R, Oliphant TE, et al (2020) SciPy 1.0: Fundamental algorithms for scientific computing in Python. Nature Methods 17:261–272. https://doi.org/10.1038/s41592-019-0686-2

Ward JH (1963) Hierarchical grouping to optimize an objective function. Journal of the American Statistical Association 58(301):236–244. https://doi.org/10.1080/01621459.1963.10500845

Wilkinson MD, Dumontier M, Aalbersberg IJJ, et al (2016) The FAIR guiding principles for scientific data management and stewardship. Scientific Data 3:160018. https://doi.org/10.1038/sdata.2016.18

689 World Bank (2026) World Bank country and lending groups.
690 https://datahelpdesk.worldbank.org/knowledgebase/articles/906519-world-bank-country-and-
691 lending-groups
692 Wurm M, Erbertseder T, Weigand M, Taubenböck H (2025) Global scaling of urban air quality. PLOS
693 ONE 20(10):e0333902. https://doi.org/10.1371/journal.pone.0333902